Human Molecular Genetics, 2016, Vol. 25, No. 20 4518–4532

doi: 10.1093/hmg/ddw280
Advance Access Publication Date: 23 August 2016
Original Article

ORIGINAL ARTICLE

Exploiting the CRISPR/Cas9 system to study alternative splicing *in vivo*: application to titin

Karine Charton[1,2], Laurence Suel[1,2], Sara F. Henriques[1,2,3], Jean-Paul Moussu[4], Matteo Bovolenta[5], Miguel Taillepierre[4], Céline Becker[4], Karelia Lipson[4] and Isabelle Richard[1,2,*]

[1]INSERM, U951, INTEGRARE research unit Evry, France, [2]Généthon, Evry, France, [3]University of Evry-Val-D'Essone, Evry, France, [4]SEAT - SErvice des Animaux Transgéniques CNRS -TAAM -phenomin UPS44 Bâtiment G 7, rue Guy Môquet 94800 Villejuif, France and [5]Department of Life Sciences and Biotechnology, University of Ferrara, Ferrara, Italy

*To whom correspondence should be addressed at: Isabelle Richard, Genethon, 1, bis rue de l'internationale, 91000 Evry, France, Tel: 33 (0)169472938; Fax: 33 (0)169472838; Email: richard@genethon.fr

Abstract

The giant protein titin is the third most abundant protein in striated muscle. Mutations in its gene are responsible for diseases affecting the cardiac and/or the skeletal muscle. Titin has been reported to be expressed in multiple isoforms with considerable variability in the I-band, ensuring the modulation of the passive mechanical properties of the sarcomere. In the M-line, only the penultimate Mex5 exon coding for the specific is7 domain has been reported to be subjected to alternative splicing. Using the CRISPR-Cas9 editing technology, we generated a mouse model where we stably prevent the expression of alternative spliced variant(s) carrying the corresponding domain. Interestingly, the suppression of the domain induces a phenotype mostly in tissues usually expressing the isoform that has been suppressed, indicating that it fulfills (a) specific function(s) in these tissues allowing a perfect adaptation of the M-line to physiological demands of different muscles.

Introduction

Alternative splicing (AS) is a post-transcriptional mechanism producing functionally diverse products from individual genes. By modulating the association of different exons, AS can determine the stability, function and/or subcellular localization of transcripts and proteins (1–7). It is used extensively by higher eukaryotes to expand the diversity of the transcriptome and proteome encoded from a defined genome, therefore explaining the apparent discrepancy between gene number and organism complexity. Indeed, recent studies indicate that 95% of the human genes are subjected to AS (8–10). Interestingly, a large number of human diseases have been associated with primary or secondary splicing defects, exemplifying the importance of AS (11).

Remarkably, AS is a major determinant of the capacity to adapt to physiological demand and of the diversity of contractile properties of the striated muscle fibre. The muscle tissue expresses some of the genes with the largest number of exons in the human genome, therefore with the highest number of possible alternative combinations. Among those, the titin gene (*TTN*) is the champion with its 363 annotated exons (12,13). This giant protein is the third most abundant protein after myosin and actin in striated muscle (13). It is an elastic protein composed of two types of folded domains (Ig-like and fibronectin type III domains) interspersed by unique sequence regions (14). The molecule spans half a sarcomere from the Z-line to the M-line (14–16) where it plays a crucial role in maintaining the integrity of the sarcomeric structural arrangement and in

Received: May 13, 2016. **Revised:** July 29, 2016. **Accepted:** August 18, 2016

generating passive muscle stiffness. Titin has been reported to be expressed in multiple isoforms in normal muscles with considerable variability in the I-band region to ensure the modulation of the passive mechanical properties of the sarcomere (17–19). In the M-line, only the penultimate Mex5 exon coding for the specific is7 domain has been reported to be subjected to AS (20). The proportion of *Titin* Mex5+ and Mex5- molecules appears to correlate with differences in the M-line fine structure that occur between type of muscles, developmental stage and species (for review (21)). Is7, a domain encased between two Ig domains, M9 and M10, is part of a binding site for calpain 3, a calcium-dependent cysteine protease implicated in limb girdle muscular dystrophy 2A when mutated (22–31). Interestingly, mutation in Mex5 was reported in Tibial Muscular Dystrophy (TMD) (32). Furthermore, this exon was reported to be abnormally spliced in myotonic dystrophy type 1 (DM1), a multisystemic disorder due to triplet expansion in the DMPK gene (33).

Investigation of the role of the is7 domain *in vivo* has been impeded by the size of the titin molecules. In this report, we took advantage of the straightforward and versatile gene editing technology based on the CRISPR-Cas9 (Clustered Regularly Interspersed Palindromic Repeats-CRISPR associated protein 9) system to precisely delete the Mex5 exon in the murine genome. Interestingly, we observed a dystrophic phenotype in the striated muscles (i.e. the *soleus* and the heart) that normally express only a Mex5+ isoform, highlighting the importance of the corresponding domain for the function of titin in these particular striated muscles.

Results

M-line titin organization and isoforms in mouse skeletal muscle

The domains of titin located in the M-band are encoded by the 6 last exons of the *Ttn* gene, called Mex1 to Mex6. Mex5 encodes the penultimate is7 domain which is reported to be alternatively spliced in skeletal muscle and is known to interact with calpain 3 (Fig. 1A) (31,34). The spatial and temporal expression of the corresponding transcript variants has not been studied in the adult mouse muscles. To characterize the expression pattern of the 2 *Ttn* variants, we first performed an RT-PCR experiment in different skeletal muscles and also in the heart of C57Bl/6 mice (Wild-type: WT) using *Ttn*-specific primers (Supplementary Material, Table S1). The results showed that the cardiac tissue expresses only *Ttn* forms including the alternative exon (Mex5+) while the skeletal muscles show different ratios of both isoforms, with the Mex5+ isoform being predominantly expressed especially in the *soleus* (Fig.1B). Quantification by real-time RT-PCR confirmed the predominance of the expression of the Mex5+ *Ttn* isoform in this muscle with 90% of the transcript whereas the other skeletal muscle samples express variable levels of Mex5+ forms (Fig. 1C).

Use of the CRISPR-Cas9 system induces Mex5 precise deletion at DNA, RNA and protein level *in vitro*

With the aim of specifically deleting the Mex5 exon of murine *Ttn*, we probed the Mex5 adjacent intronic regions of the mouse *Ttn* gene sequence from the Mouse July 2007 NCBI37/mm9 assembly, using the freely available ZiFit Targeter software. Three upstream (designated g8, g9 and g10) and two downstream (g2 and g5) truncated single guide RNAs (sgRNA) (35) following the N_{18}NGG rule were selected after considering the absence of overlapping SNPs in the murine genome as determined on dbSNP and their potential off-targets (Table 1, Fig. 2A). These sgRNAs were first tested *in vitro* in pairs to determine the most efficient combinations. The expected sizes of the deletion of the different pairs are between 380 and 670 nucleotides. Pairs of the selected sgRNA and a streptococcus pyogenes (sp) Cas9-GFP-encoding plasmid were co-transfected in the mouse cell line NIH3T3. Forty eight hours after transfection, DNA was extracted and a PCR analysis was performed to detect deletion and inversion. The results showed that the expected deletion of the Mex5 exon was obtained only with the combinations g8-g2 and g8-g5 which correspond to the 2 smaller distances between guides of all combinations (Fig. 2B). We also observed that inversion of the Mex5 exon occurred for all the pairs of sgRNAs but again with apparently a higher efficacy with the g8-g2 and g8-g5 pairs (Fig. 2C). With respect to these results, the 2 pairs g8-g2 and g8-g5 were selected for the subsequent experiments.

The NIH3T3 cell line does not express titin at the RNA level, preventing the validation of the deletion on the actual skipping-out of Mex5 exon at messenger level. Therefore, we next tested the efficiency of the g8-g2 and g8-g5 sgRNA pairs on the mouse myogenic C2 cell line that we previously validated as expressing Mex5+ *Ttn* transcripts already at myoblast stage. The sgRNA pairs were co-transfected with Cas9-GFP and 48 hours after, DNA and RNA were extracted from GFP positive cells selected by flow cytometry because of reduced transfection efficiency in these cells. Analysis by PCR and sequencing of the selected bands at the DNA level showed the deletion of Mex5 with the two sgRNA pairs, consistent with the results obtained in NIH3T3 (Fig. 3A). Inversions were also detected (data not shown). The result obtained at the RNA level by RT-PCR with primers in Mex4 and Mex6 and by sequencing of the excised bands showed the perfect excision of the Mex5 exon (Fig. 3B), indicating that the deletion does not disturb the correct usage of the splicing sites in Mex4 and Mex6 and allows the expression of an in-frame is7$^-$ *Ttn* variant.

We performed an additional *in vitro* experiment to observe the consequence of Mex5 DNA deletion on the translation of titin. Due to the huge size of titin that would prevent detecting the deletion of the 11 kDa is7 among the $\sim$ 3 MDa of the protein even with a high resolution Western Blot (WB), we relied on the use of a mouse *Ttn* minigene coding for the 5 last exons/introns. This minigene was co-transfected with the sgRNAs and the Cas9-GFP and analyses performed 48 hours after transfection on total cells. A genomic PCR showed a lower band corresponding to the Mex5 deletion with both pairs (Fig. 3C). A RT-PCR performed with primers specific to the transcript expressed from the minigene revealed the predominant presence of the Mex5- isoform, consistent with the results obtained in the previous experiments (Fig. 3D). A WB analysis performed with a GFP antibody and an antibody directed against V5 showed, both in the untransfected and Cas9-only transfected cells, a 74 kDa protein band corresponding to the expected size for the domains of titin expressed from the minigene and a 64 kDa band that correspond to the expected size of the is7$^-$ Ttn isoform with both sgRNA pairs (Fig. 3E). These data indicated that these conditions induce a Mex5 DNA deletion which can lead to the generation of a protein without the is7 domain.

Creation of a mouse model with specific deletion of the titin Mex5 using CRISPR/Cas9 system

After *in vitro* validation, the g8-g5 sgRNA pair was selected for the generation of a mouse model on the basis of its efficiency to

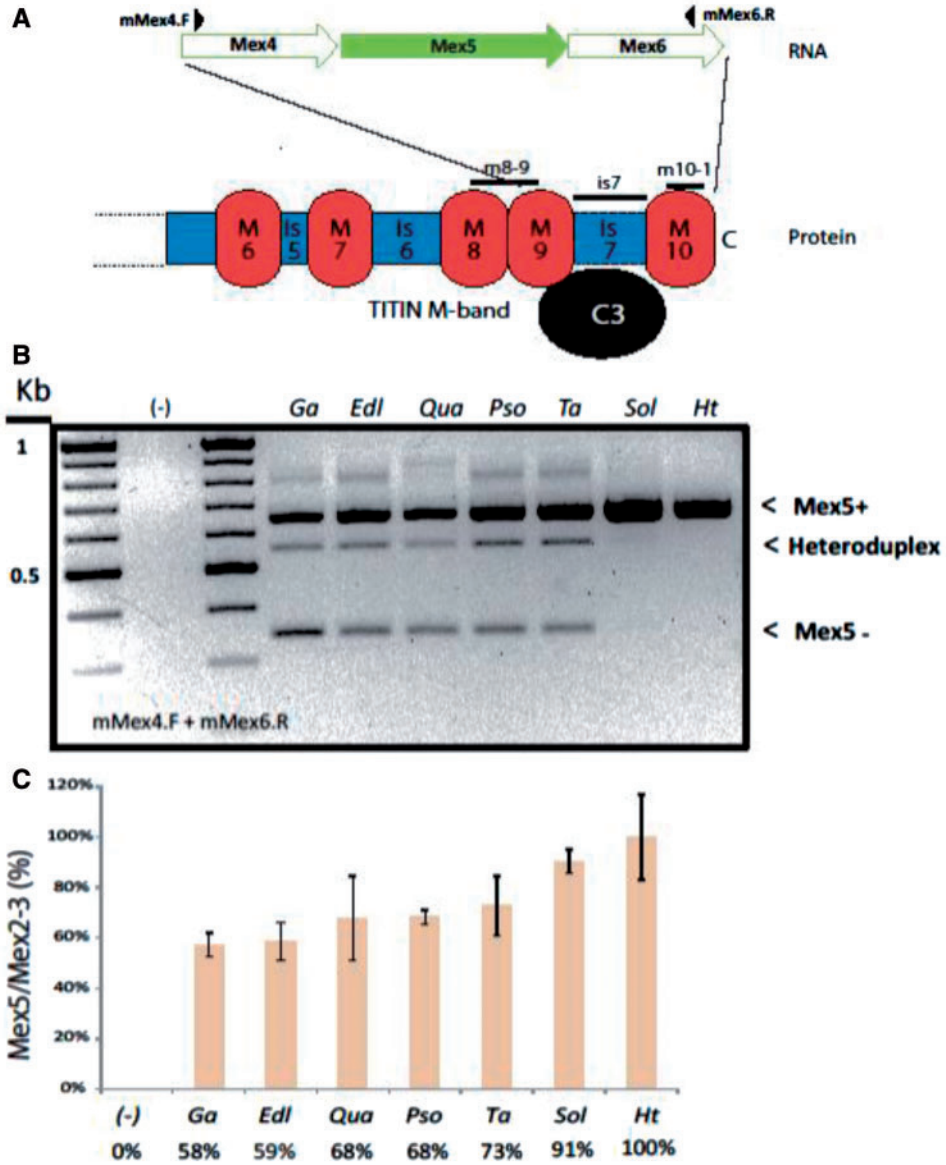

Figure 1. The M-line titin and its isoforms in mouse skeletal muscle. (**A**) Arrangement of the 3' last exons (Mex4 to Mex6) of titin and of the C-terminus of the protein. The primers used for RT-PCR experiments are represented as black arrows along the messenger RNA. The locations of the epitopes of the different antibodies used in this study (m8-9, is7 and m10-1) are depicted in black above the protein representation. The calpain 3 binding site is shown below the Titin protein. (**B**) RT-PCR on mouse skeletal and cardiac muscles using mMex3.F and mMex6.R primers showing the Mex5+/Mex5- titin isoforms in different mouse skeletal muscles. A heteroduplex DNA band is visible on all lines where Mex5- is expressed. (-) = H_2O negative control. Ga = *gastrocnemius*, Edl = *extensor dgitorum longus*, Qua= *quadriceps*, Pso = *psoas*, Ta = *tibialis anterior*, Sol = *soleus*, Ht = *heart*. (**C**) Quantification by qRT-PCR of Mex5+ isoform depending on the muscle in % with respect to an qRT-PCR amplifying the total of titin RNA isoforms (primers located in titin Mex2-3) (-)=H_2O negative control.

generate a precise Mex5 exon deletion and on reduced off-target effects for the g5 compared to the g2 sgRNA as predicted by the ZiFit platform (Table 1). Indeed, the g2 is predicted to target potentially three 2-bases-mismatched sequences despite the fact that g5 has only one (none of them has 1-base mismatched target site) and one of the g2 mismatched targets was predicted to occur in the coding sequence of the *Lrrc37* gene. The sgRNAs g5 potential target site is in an intergenic region of chromosome 14 whereas the three predicted g8 2-mismatched off-target sites are in non-coding sequence of genes on chromosome 4, 9 and 8 (Table 1). We then tested the g5 and g8 potential off-target effects *in vitro* after transfection and flow-sorting of Cas9-GFP-positive C2 cells. The extracted DNA was amplified using specific oligonucleotides covering each potential off-target site (Supplementary Material, Table S2) and the PCR products were subjected to T7 endonuclease 1-mediated cleavage after denaturation-renaturation. No targeting event was detected for any of these predicted sites (Fig. 4A).

Different concentrations of a capped and polyadenylated spCas9 mRNA (5' methylcytidine, pseudouridine) and *in vitro* transcribed sgRNAs were co-microinjected in B6/CBA one-day zygotes that were reimplanted in pseudopregnant mice following the described protocol of Yang and colleagues (36). After 3 weeks, from the total of 224 injected and reimplanted zygotes, 19 pups were born (Table 2). Genotyping of the progeny was performed by PCR on tail DNA and revealed different editing events. Five pups (#3, 4, 8, 12 and 19) presented variable level of deletions of slightly different sizes with 2 animals (#8 and 19)

Table 1. Single guide RNA sequences selected using Zifit software and potential off-target predictions for ≤ 2-base mismatches. The targeted regions were checked on UCSC genome browser database (http://genome.ucsc.edu/)

Potential off-target site	Chr	location	Strand	Position	Mismatch #1	Mismatch #2	GENE
sgRNA8 - GAGCATAGCAGATACACG	Chr2	5′	+				*Ttn*
1	Chr9		–	98701661	A>C	A>C	*E330023G01Rik* (3′UTR)
2	Chr4		–	124510706	G>A	C>G	*Mtf1* (intron)
3	Chr8		+	64283639	T>G	C>G	*Palld* (intron)
sgRNA5 -GAACGATGCCATGCTAGG	Chr2	5′	–				*Ttn*
1	Chr14		–	104631251	C>G	T>C	Intergenic
sgRNA2 - GAGAGTCTCGACAACGTG	Chr2	3′	–				*Ttn*
1	Chr6		+	87300098	G>A	A>T	*Gkn1* (intron)
2	Chr6		+	126494220	C>G	C>G	Intergenic
3	Chr11		+	103407062	C>G	A>T	*Gm884* (exon)
sgRNA9 - GCAGCTGCTAGAAGTTGC	Chr2	3′	+				*Ttn*

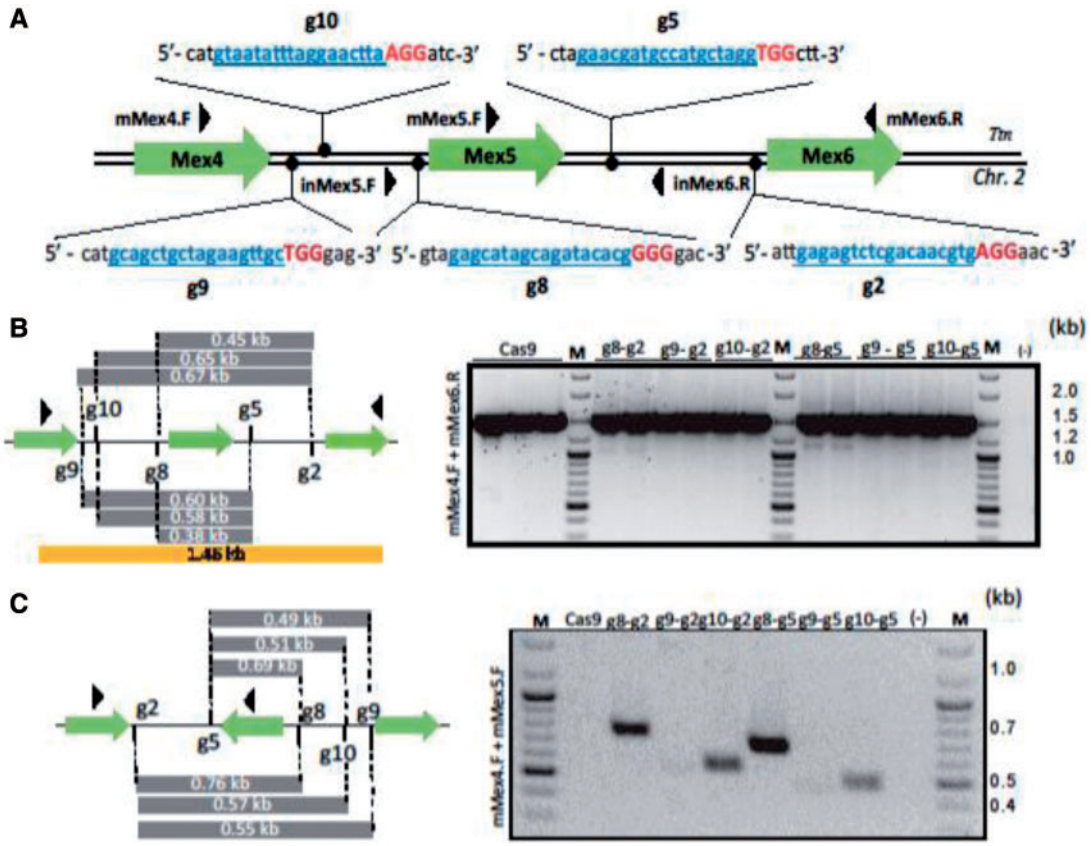

Figure 2. Efficiency of single guide RNAs in NIH3T3 cells at DNA level. (**A**) Schematic illustration showing the sequences and locations of the sgRNAs (g2, g5, g8, g9, g10) along the mouse genomic region of *TTN* Mex4 to Mex6. Exons are depicted as big arrows. The sgRNA sequences are indicated from 5' to 3' and their respective targeted genomic strand is indicated by a small dot. The target sequences are in blue and the PAM in red capital letters. The primers used for the analysis of deletion and inversion are indicated by small arrowheads. (**B**) Genomic PCR analysis of the deletion efficiency of all combinations of sgRNA (one upstream and one downstream Mex5) after transfection of NIH3T3 cells. **Left panel**: schema indicating the expected size of the DNA deletions according to the utilized sgRNA. **Right panel**: gel electrophoresis of PCR products obtained using primers across the expected deletions (mMex4.F and mMex6.R). Cas9 = Cells transfected with only a Cas9-GFP plasmid, M = Molecular weight marker. (-) = H_2O. (**C**) PCR analysis using primers that allow the detection of DNA inversions after transfection of NIH3T3 cells. **Left panel**: schema indicating the expected size obtained after DNA inversions depending on the sgRNA locations. Cas9= Cells transfected with a Cas9-GFP plasmid only, M = Molecular weight marker, (-) = H_2O. **Right panel**: gel electrophoresis of PCR products obtained using the mMex4F and mMex5F primers for all sgRNA combinations on NIH3T3 DNA.

showing apparent complete deletion on both alleles. One addition animal (#6) presented a partial deletion and 3 (#13, 14 and 17) inversions (Fig. 4B). The events were further investigated by sequencing analysis on isolated bands, which confirmed that the double strand break introduced by Cas9 had been repaired randomly, giving rise to slightly different deletion events depending on the sequenced founder DNA and in accordance with the different sizes seen on gels (Fig. 4C). We then investigated the off-target effects in muscle samples of the 5 pups showing correct deletion of the Mex5 exon (Table 2). Contrary to what was observed in cells, T7E1 cleavage occurred in the potential targeted sequence on the chromosome 9 for 3 mice out

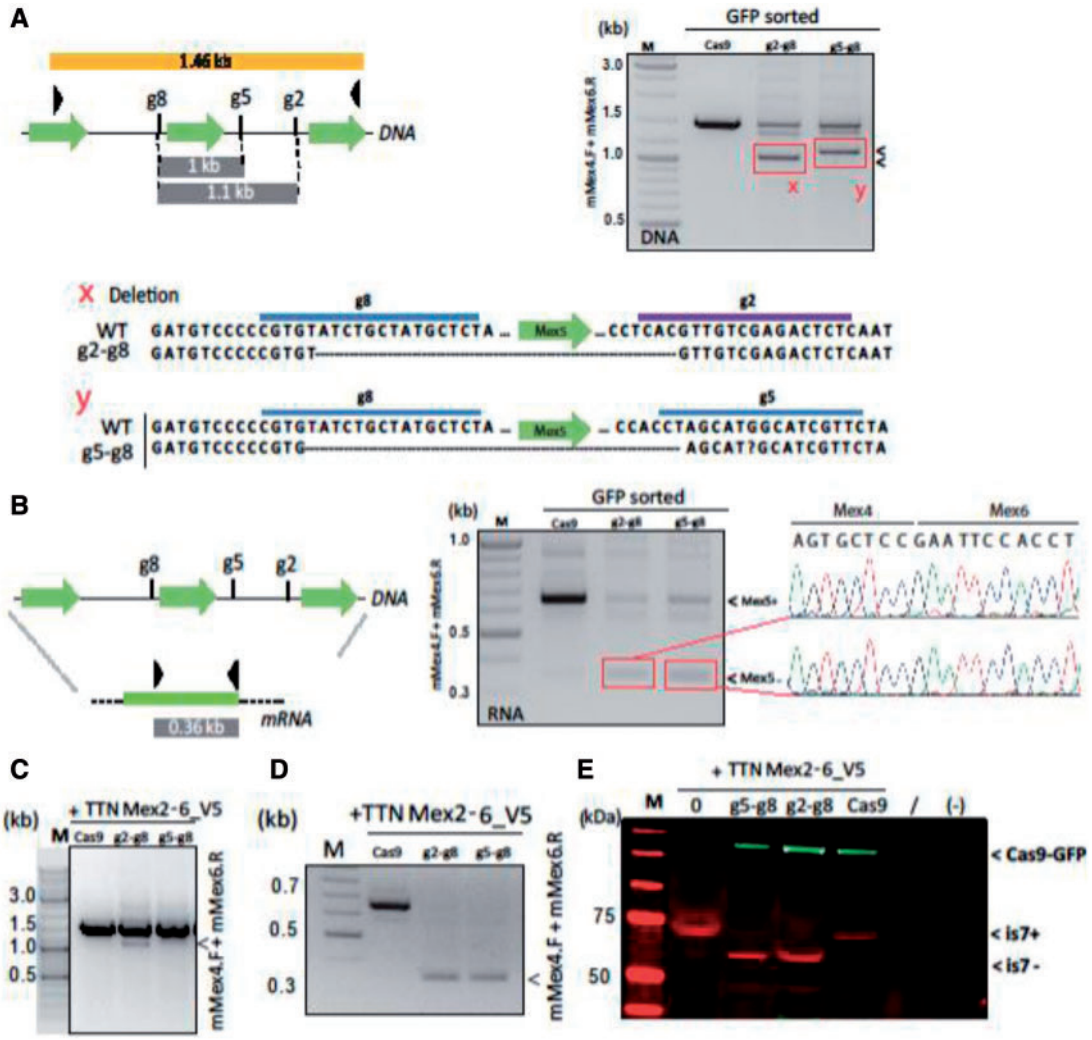

Figure 3. Analysis of the consequences of Mex5 deletion at messenger and protein levels. (**A**) DNA deletion analysis after transfection of the Cas9-GFP plasmid and the selected sgRNAs on the myogenic C2 cell line. The cells were sorted by FACS according to the intensity of GFP fluorescence. **Left panel**: schema indicating the expected size of the PCR according to the utilized sgRNA. **Right panel**: gel electrophoresis of PCR products obtained using primers across the expected DNA deletion. The corresponding Wild-type (WT) and deleted sequences are shown below. (**B**) RNA deletion analysis after transfection of the Cas9-GFP plasmid and the selected sgRNAs on the myogenic C2 cell line. The cells were sorted by FACS on the intensity of GFP fluorescence. **Left panel**: schema indicating the expected size of the Mex5 deletion at the mRNA level. **Middle panel**: gel electrophoresis of cDNA using the same primers. **Right panel**: chromatograms showing the deletion of Mex5 at RNA level. (**C**) Gel electrophoresis of PCR products obtained using primers to detect the DNA deletion in HER911 cells transfected with the Cas9-GFP plasmid, the selected sgRNAs and a mouse *ttn* minigene from Mex2 to Mex6. (**D**) Gel electrophoresis of RT-PCR products obtained using primers to detect the cDNA deletion. (**E**) Western blot analysis for detection of Cas9-GFP (in green) and the titin miniprotein (in red); Cas9 = cells transfected with only the Cas9-GFP plasmid, 0 = no sgRNA, M = Molecular weight marker, (-) = non transfected cells.

of 5 (Fig. 4D). We validated by sequencing that this observation corresponds to off-target editing and is not due to the presence of an SNP between the C57Bl/6 and CBA genomes.

We selected two founder animals for crossbreeding, in order to validate transmission to the offspring and to perform a molecular characterization of the F1 generation. DNA was extracted from the *gastrocnemius* muscle of the titin$^{Mex5-/Mex5-}$ F1 mice at 4 months of age and the deletion of the Mex5 *Ttn* exon was validated by PCR and sequencing (Fig. 5A). A correct Mendelian transmission ratio was observed as among the 224 offsprings engendered from HE crosses, 56 (25%), 95 (42%) and 73 (32%) correspond to WT, HE and HO genotypes, respectively ($P > 0.05$). The absence of the Mex5 sequence at the RNA level was verified, indicating a correct splicing of Mex5 *Ttn* RNA (Fig. 5B). Quantitative RT-PCR of the Mex5 exon was performed on different muscles (*Heart, Sol, Ga, Qua, Ta*) and showed complete deletion of the Mex5 exon in all tested muscles (Fig. 5C). To analyse the consequences at the protein level by Western blot, we performed a protein extraction by sub-fractionation, a technique that we previously validated as generating a reproducible profile of titin fragments (24,25). An antibody directed specifically against the is7 domain showed loss of the expected fragment at 45 kDa which corresponds to the C-term part of titin containing the is7 domain encoded by Mex5 (Fig. 5D). Finally, specific immunostainings of titin domains on muscle sections showed the complete loss of the specific alternative is7 domain in the *gastrocnemius* of the titin$^{Mex5-/Mex5-}$ mouse but the correct integration of the full-length titin in the sarcomere and the presence of the last domains of titin on each sides of the deletion (m8-9 and m10-1) (Fig. 5E).

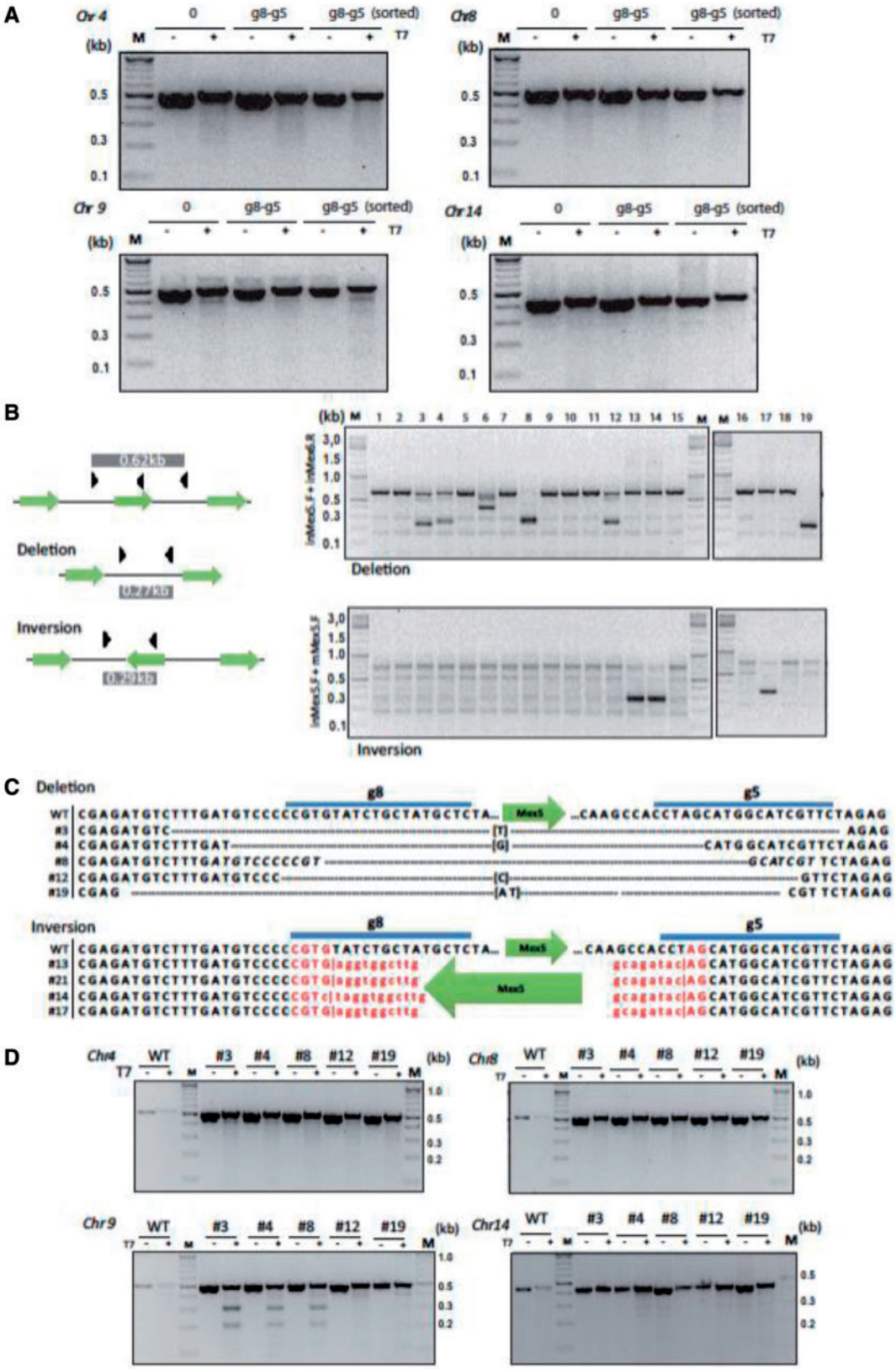

Figure 4. Generation and molecular analysis of the titin$^{Mex5-/Mex5-}$ mice. (**A**) Off-target analysis on transfected C2 cells. The PCR products were subjected to T7 cleavage assay using oligonucleotides specific for the predicted chr4, 8, 9 and 14 off-target sites. (**B**) Genotyping on tail DNA of the F0 mice. **Left panel**: possible scenarios. **Right panel**: PCR for deletions or inversions on tail DNA of mice 1 to 21. (**C**) Genomic deletion at the targeted site of all deleted or inverted F0 mice. Mouse #8 carries 2 different deletions, the alternative sequence is written in italic. The uncertain sequence is written in brackets. (**D**) Off-target analysis for the mice showing a deletion of Mex5. The PCR products were subjected to T7 cleavage assay using oligonucleotides specific for the to the predicted chromosome 4, 8, 9 and 14 off-target sites.

Table 2. Summary of microinjection experiments (conditions and results). In brackets, numbering of mice presented in Fig. 4.

Cas9 / sgRNA concentrations used	Nb. of transferred zygotes	Nb. of pups	Number of genetic modifications at the locus	Number of deletions at the locus	Number of inversions at the locus
50 ng/µl Cas9 20 ng/µl sgRNA	80	6 (#1 to #6)	2/6	3/6 but one partial	0/6
20 ng/µl Cas9 10 ng/µl sgRNA	68	9 (#7 to #15)	4/9	2/9	2/9
5 ng/µl Cas9 10 ng/µl sgRNA	76	4 (#16 to #19)	2/4	1/4	1/4
Total	**224**	**19**	**8/19 (47%)**	**6/19 (32%)**	**3/19 (16%)**

Effect of titin domain is7 exclusion in mouse muscles

The consequences of the deletion of murine titin is7 domain were evaluated on different muscles and heart. First, the weight of the titin$^{Mex5-/Mex5-}$ mice and their different muscles (*Ta, Ht, Ga*, and *Sol*) did not show any significant difference as evaluated at 4 months of age (Supplementary Material, Fig. S1A and B). Interestingly, the skeletal muscle expressing nearly exclusively the titin Mex5+ isoform in a wild-type manner (i.e. *Sol*, see Fig. 1B) showed a dystrophic pattern already at 4 months of age (Fig. 6A). Conversely, no dystrophic pattern was shown in the muscles which normally express both Mex5 *Ttn* isoforms at that age (*Ta, Qua* and *Ga)* (Fig. 6A, Supplementary Material, Fig. S1C). The main pathological features seen in the *Soleus* muscle are a high number of fibres with centrally located nuclei and a large number of necrotic fibres (Fig. 6A). We confirmed that these abnormalities correspond to a dystrophic process since they correlated with an increase of mi-RNA31 (37) and mi-RNA142-3p (38), two microRNAs reflecting the presence of a regeneration process and inflammatory infiltrates, respectively (Fig. 6B). At 6 months of age, all muscles displayed a dystrophic impairment, indicating a progression of the pathology, with notably the *Soleus* being the most sensitive to develop a phenotype (Supplementary Material, Fig. S2A). The functional status of the *Sol* muscle was tested *in vitro* and the specific force generated after tetanic stimulation was measured. The *Sol* force remains normal in the mice titin$^{Mex5-/Mex5}$ even if this muscle shows a dystrophic pattern (Fig. 6C). Moreover, the contractile parameters (contraction slope and half relaxation time) are not different (data not shown).

The histology of the cardiac tissue (also expressing exclusively the *Ttn* Mex5+ isoform) was examined. The HPS-stained cross-sections of titin$^{Mex5-/Mex5-}$ hearts display a marked pathology noticeable as early as 2 months of age (data not shown) and with large areas of damaged tissue both at 4 and 6 months of age with a progression of 5 to 20% of total fibrosis heart area. (Fig. 6D, Supplementary Material, Fig. S2B). Consistently, Sirius red staining revealed extensive areas of interstitial fibrosis. Quantification of collagen areas confirmed these myocardial alterations (Fig. 6D).

To study the consequences of at the molecular level, we investigated a number of interacting partners of the C-ter titin. First, we performed quantification of expression of Calpain 3, a well-known Titin is7 domain partner, by qRT-PCR in different muscles (*Heart, Sol, Ga, Qua, Ta)* (Fig. 7A) and WB in *Ga* muscle (Fig. 7B). Interestingly, even though *Capn3* messenger expression is not modified, we demonstrated an important decrease of Capn3 at the protein level, suggesting possible protein instability due to the is7 domain loss in this mouse model. A calpain 3 staining in muscle fibres revealed no modification of immunostaining compared to WT (Fig. 7C). Second, MURF1 and MURF2 which are partners of titin in the M-line upstream of is7 show no difference at the expression level (Supplementary Material, Fig. S3A) or mis-localization in the Titin$^{Mex5-/Mex5-}$ muscle (Supplementary Material, Fig. S3B and C). Third, a partner of titin downstream of is7, the M10-interacting-protein obscurin (OBSCN) was analysed without showing any difference (Supplementary Material, Fig. S3D). Finally, we also considered the expression of CARP in this model since CARP was reported to respond to titin alteration. CARP shows no overexpression at the protein level in muscle compared to WT (Supplementary Material, Fig. S3E).

Discussion

The CRISPR-Cas9 system is revolutionizing the gene editing field thanks to its simplicity, efficiency and speed of generating animal models. By microinjection of CRISPR-Cas9 components that include sgRNA that target both sides of an in-frame exon in one-cell stage embryos, we were able to quickly generate a mouse model that expresses a specific alternatively spliced titin variant(s). To our knowledge, this report is the first where the CRISPR-Cas9 technology has been used to functionally assess a natural occurring protein variant *in vivo*. The interest of *in vivo* investigation of AS by CRISPR-Cas9 has been illustrated by the apparition of a phenotype in tissues expressing usually at high levels the isoform that has been suppressed. Interestingly, although AS in titin is quite prevalent, the only previously reported investigation of AS *in vivo* was through the knock-out of RBM20, a splicing regulator targeting also other genes (38). Therefore, our model is the first precise and specific model of titin splicing.

Previous studies investigating the *in vivo* consequences of alternative splicing have relied mostly on classical genetic engineering of the murine genome by transgenesis (performed for the Titin N2B and PEVK domains (39,40), or in a few cases, using exon-skipping in adult animals (for examples (41–45)). Alternatively, the modulation of a splicing has involved manipulation of a splicing regulator as performed for RBM20 (46) or MBNL1 (47). All these techniques have their own limitations in terms of efficacy, time demand or the types of events that can be evaluated. Not surprisingly, *in vivo* evaluation of alternative splicing variants has been limited to specific cases, mostly related to human diseases. Interestingly, the versatility of the CRISPR-Cas9 technology is opening a full range of new possibilities for the *in vivo* study of AS. Creation of an exon deletion does not require a DNA repair template and mimics a splicing-out event that maintains the RNA exon organization. Moreover, the versatility of the technique as demonstrated in previous examples (48–50) is a tremendous advantage in the case of huge genes with multiple variants such as titin. It is possible to envision a detailed analysis of spliced variants by removing exons at different places along the entire length of the gene one at a time or by analysing variants with exons spread along a large piece of DNA. Undesired genetic modifications such as off-target

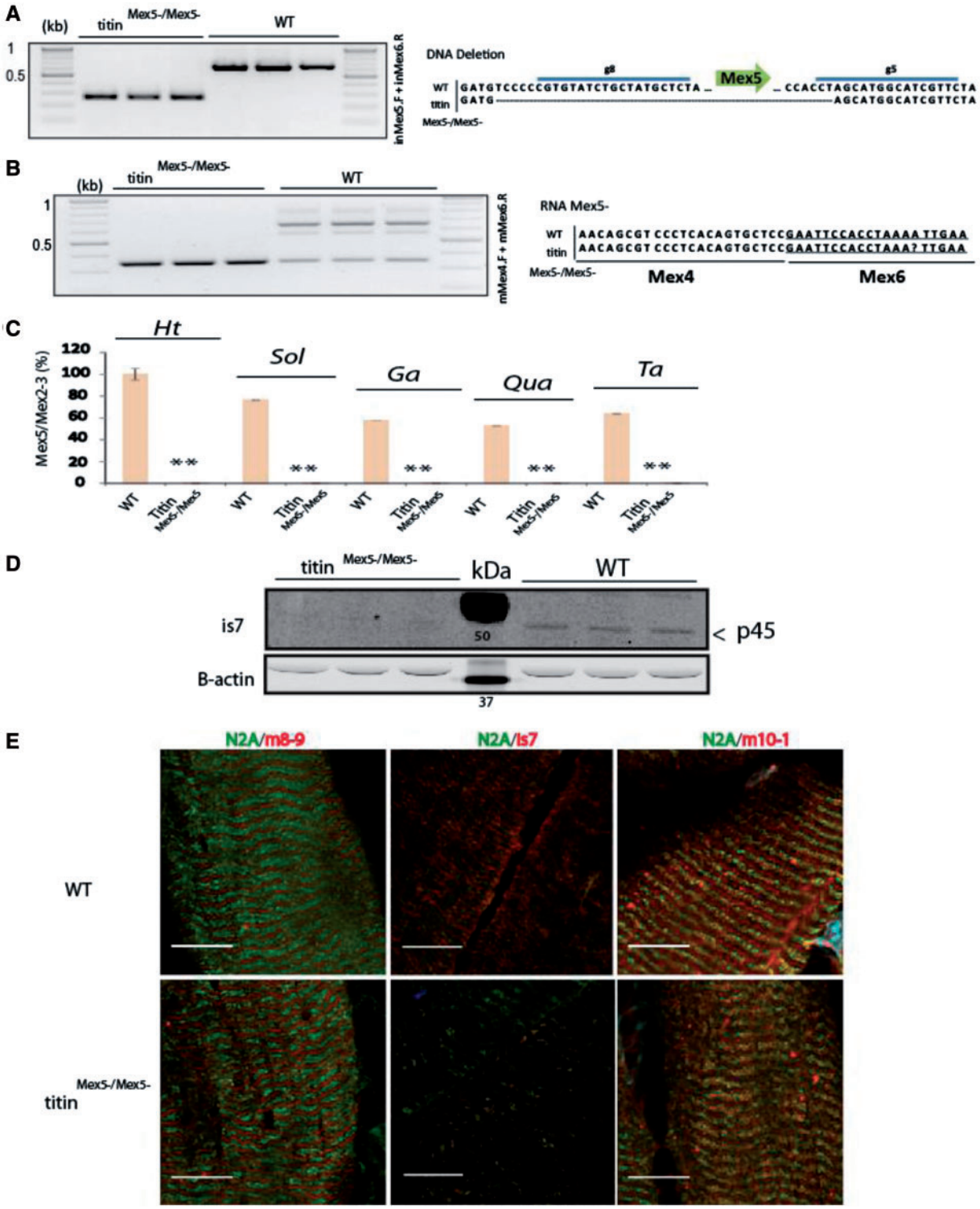

Figure 5. Molecular validation at muscle level of the F1 titin$^{Mex5-/Mex5-}$ mice . (**A**) Specific Mex5 PCR (Mex3 to Mex6) on DNA extracted from *gastrocnemius* muscle of the F1 mice (4 month-old males) and sequencing ($n = 3$). (**B**) *Titin* RT-PCR on *gastrocnemius* and sequencing ($n = 3$). (**C**) Mex5 quantification normalized by titin Mex2-3 level on cDNA obtained from different muscles (*Heart*, *Sol*, *Ga*, *Qua*, *Ta*) ($n = 3$), **= $p < 0.01$. (**D**) WB on titin fragment using the cytoskeletal fraction of the *gastrocnemius* muscles of WT and titin$^{Mex5-/Mex5-}$ mice ($n = 3$). Staining was performed using is7 antibody (in green). α-Actin was used for normalization (in red). (**E**) Titin immunostaining on *gastrocnemius* longitudinal section using m8-9, is7 and m10-1 (in red) and N2A (in green) antibodies for WT and titin$^{Mex5-/Mex5-}$. Scale bar = 10 μm.

cleavage or inversion are easily segregated by backcrossing and careful genotyping. Moreover, the use of newer versions of Cas9 which exhibit reduced off-target cleavage (51,52) would also help to reduce non-specific genomic editing.

Through this proof-of-concept experiment, we learned that the deletion of the titin is7 domain is not embryonic lethal and therefore that the region is dispensable during development even though the is7+ seems to be the embryonic form of titin

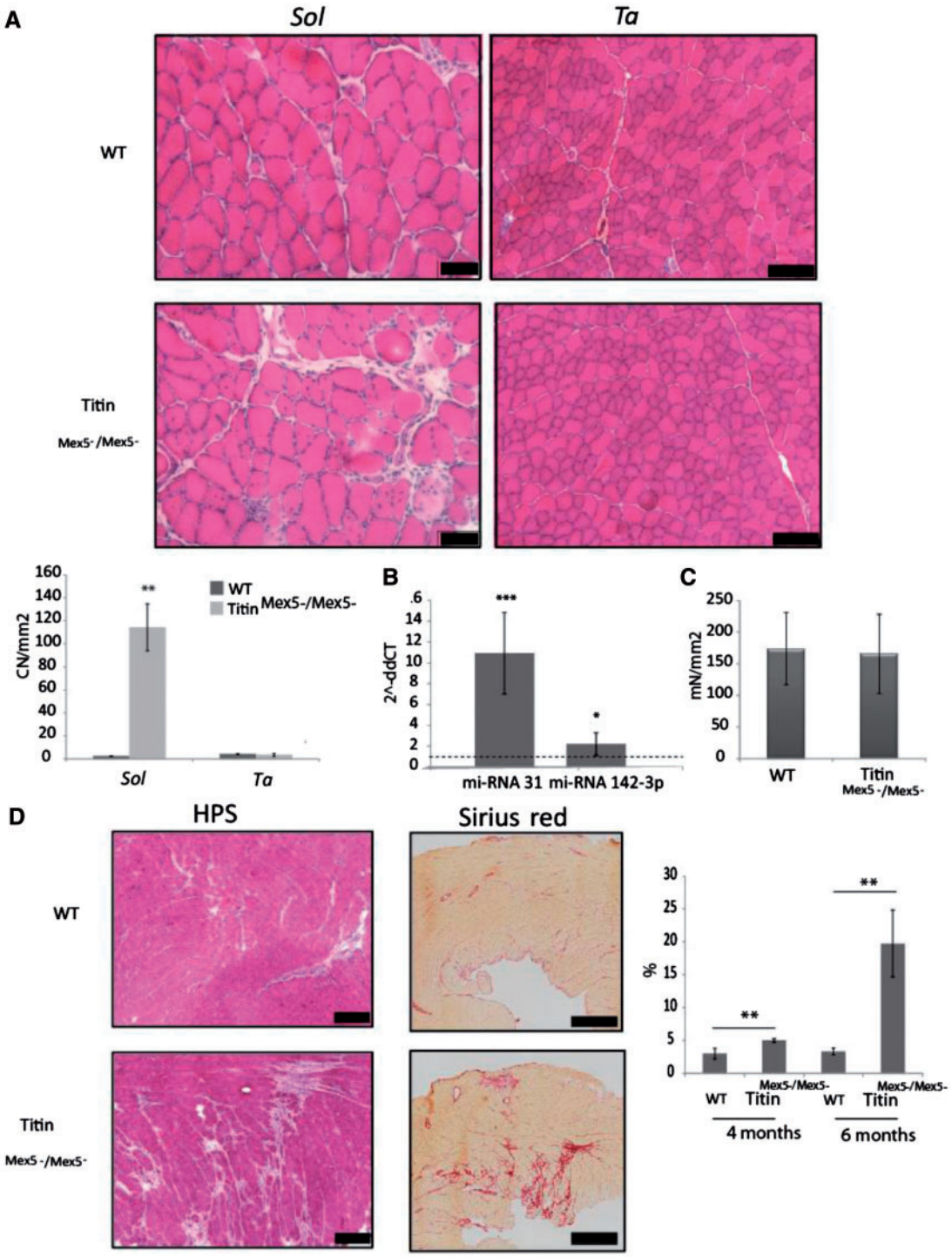

Figure 6. Muscle phenotype of the titin$^{Mex5-/Mex5-}$ F1 mice at 4 months of age. (**A**) Upper panel: Transverse section of the *Sol* (Scale bar = 50 μm), *Ta* (Scale bar = 150 μm) of the 4 month-old male mice WT and titin$^{Mex5-/Mex5-}$. Lower panel: Centronucleation quantification in the *Sol* and *Ta* muscles. **=$p < 0.01$. (CN/mm^2 = Centronucleated fibres/mm^2). (**B**) Normalized quantification of mi-RNA31 and mi-RNA142-3p in *soleus* muscle represented in $2^{-\Delta\Delta CT}$ by comparison with WT samples (dashed line). (**C**) Measure of *Soleus* specific force at 4 months of age ($n = 8$). Tetanic specific force was measured at L0 in WT and titin$^{Mex5-/Mex5-}$ animals. (**D**) Transverse section of the heart (Scale bar = 150 μm) (left) and staining of the fibrosis with sirius red (Scale bar = 500 μm) (middle). Fibrosis quantification in the *heart* in % of total surface at 4 and 6 months-old (right). *=$p < 0.05$, **=$p < 0.01$, ***=$p < 0.001$.

(20). The fact that the splicing-out occurs after birth suggests that modulation of the domain inclusion/exclusion is required for a specific purpose in relation with muscle activity (20). Of note, the level of splicing-out of this exon was shown to be variable depending on the models, indicating another level of regulation. Since the suppression of the domain induces heart failure and muscle dystrophy selectively in one specific muscle (*Soleus*), it can be concluded that it fulfils (a) specific function(s) in these tissues. It is of interest to compare the phenotype of this model with the mice carrying the FINmaj mutation. This

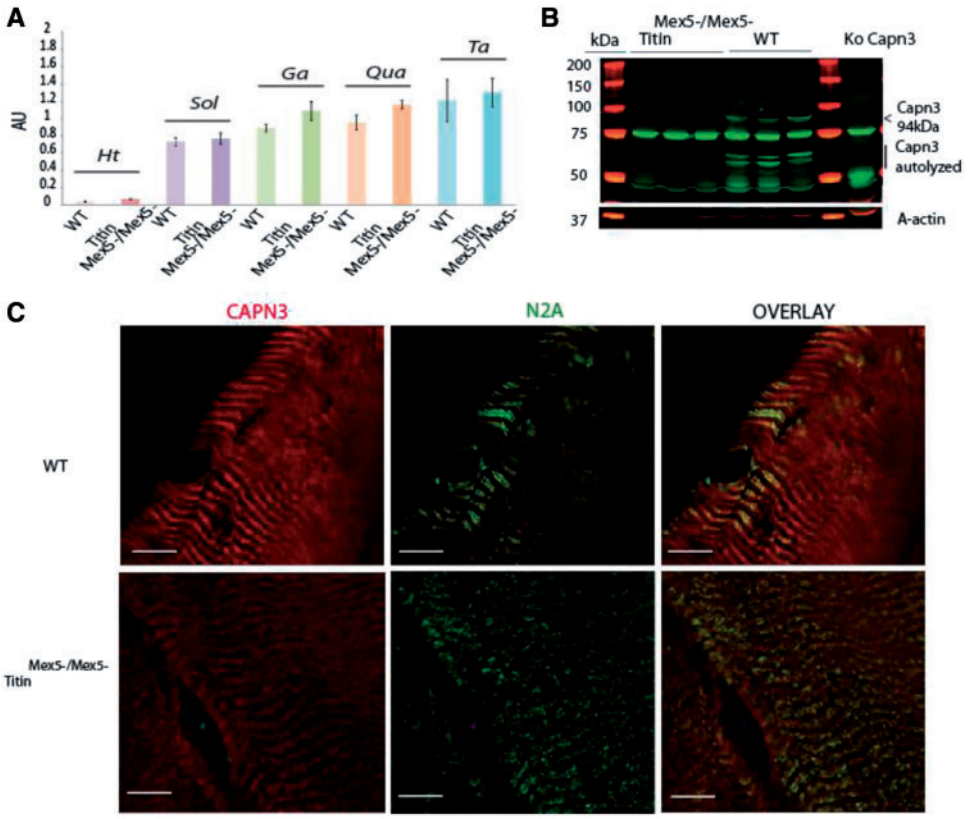

Figure 7. Downstream effect of TTN is7 deletion on calpain 3: (**A**) Analysis of Calpain 3 expression reported on P0 by quantitative RT-PCR in different muscles (*Heart, Sol, Ga, Qua, Ta*) of WT and titin$^{Mex5-/Mex5-}$mice ($n = 3$) (AU = Arbitrary Unit). (**B**) Analysis of Calpain 3 expression (in green) by WB in *Gastrocnemius* muscles of WT and titin$^{Mex5-/Mex5-}$. α-actin was used for normalization (in red). (**C**) CAPN3 immunostaining (in red) and N2A (in green) on TA longitudinal section for WT and titin$^{Mex5-/Mex5-}$. Scale bar = 10 μm.

prevalent mutation is at the origin of the phenotype of Tibial Muscular Dystrophy when present on one allele and Limb Girdle Muscular Dystrophy type 2J when at present on both alleles (53). We showed that one of the consequences of the mutation is a secondary loss of the last M-line domains of titin from is6/M8 area to the C-terminus therefore larger but including the is7 domain. Interestingly, only a small proportion (3.2%) of homozygous FINmaj mice survives to the perinatal period (24). This lethality which is not seen in the Titin$^{Mex5-/Mex5-}$ model could therefore be related to a specific role in the cardiac tissue of the additional missing parts of titin. However, the muscles demonstrated to be mostly affected in the mouse model carrying the FINmaj mutation at homozygous state are the same than in the Titin$^{Mex5-/Mex5-}$ model (24), suggesting a commonality of pathological pathway.

The is7 domain is a unique region of titin located between 2 Ig-like domains known to be involved in the primary mechanism of titin stretching (54). It has no homology with other protein domains and serine comprises more than 30% of its amino acids. Since serine is known to confer flexibility in a peptide chain, this domain may serve as a linker between the 2 Ig-domains. Consequently, the presence of is7 would increase the flexibility of the N-terminus of titin in the M-band. This may have consequences at a mechanical level, allowing a better resistance to constraints both along the lateral and longitudinal axes. This flexibility would also allow different structural conformations. It has previously been shown by electron microscopy that the M-line structure is variable according to developmental stage, functional state and muscle type (55–58). Furthermore, it was suggested this may correspond to the AS of Mex5 (20). The presence of this particular domain is7 may also change the configuration of protein interactions within the M-band. Of importance, is7 is known to support only one protein interaction which is with the calpain3 protease. However, the very weak expression of calpain 3 in mouse heart (59) does not support the idea that the apparition of the phenotype in this tissue is related to the loss of this interaction. We cannot exclude, of course, that the origin of the phenotype would be different between the *soleus* and the heart and this would require further investigations. In muscles, CAPN3 demonstrated protein instability due to the is7 domain deletion, which indicates a specific role of the interaction with this domain in preventing autolytic cleavage of calpain 3 as previously demonstrated for the N2A region (30,60). Nevertheless, this instability does not induce calpain-3-mediated secondary loss of the C-ter titin at the known cleavage sites since immunofluorescence experiments indicated the conservation of the M10 positive staining. There was no consequence either on CARP, a calpain 3 substrate present in the I-band and previously shown to be upregulated in different cardiac conditions (61).

Modulation of the presence of is7 can also have an impact on other interactions through modification of the alignment of the different proteins present in the M-line. For example, this region plays a role as a scaffold for metabolic enzymes, especially creatine kinase. This point is of interest since both the heart and the *soleus* muscles have a predominant aerobic metabolism. Interestingly, other important components of the M-band sarcomere such as obscurin and the myomesin proteins

are also subjected to AS according to developmental stages or types of muscles. Therefore, the modulation of this domain would generate M-line sarcomere with different structure and quality, allowing a perfect adaptation to the physiological demands of different muscles.

To clarify between all these hypotheses, a better understanding of the structure of the M-line sarcomere and the interplays between all its constituents is mandatory. This would permit a more precise definition of the role of the is7 domain in the heart and skeletal muscle physiology and the reasons underlying its alternative splicing.

Materials and Methods

Single guide (sgRNA) design

The ZiFiT online platform (http://zifit.partners.org/ZiFiT/) (62,63) was used to design truncated sgRNAs (N_{18}NGG) (35) using the murine genomic sequence around Mex5 based on the available guidelines on CRISPR design (64). The sequences of the sgRNAs were aligned to the mouse genome (NCBIm37/mm9 Assembly) using the UCSC online portal (https://genome.ucsc.edu/) to define whether they are located within coding sequences and to exclude the presence of SNP.

Cloning and plasmid construction

The Cas9-expressing pMJ920 plasmid carrying codon-optimized spCas9 fused with a GFP reporter gene under the transcriptional control of the CMV promoter and the sgRNA expression MLM3636 plasmid carrying a U6 promoter were a gift from Jennifer Doudna (Addgene plasmids #42234) and from Keith Joung (Addgene plasmid #43860) (65). Oligonucleotides corresponding to the sgRNAs sequences were cloned into MLM3636 between BsmBI sites and the corresponding plasmids were sequence-verified (Beckman Coulter). The TTN-Mex2-6_V5 minigene (V5/His6-tagged is6–M10_V5 is7^{+}) was described previously (66) and consists of a mouse wild-type *Ttn* genomic fragment covering the 5 last exons of titin cloned into pcDNA3.1V5 (ThermoFisher Scientific).

Cell culture and transfections

Mouse NIH3T3, myogenic C2 and human embryonic retinoblast HER911 cell lines were obtained from the American Type Culture Collection, and maintained at 37 °C and 5% CO_2 in Dulbecco's modified Eagle's medium (DMEM) supplemented with 10% Fetal Bovine calf Serum and 10 µg/ml of Gentamicin (Gibco), plus Minimum Essential Medium (Gibco) for HER911 cells. A day before transfection, cells were plated in 6 well-plates to reach 60–70% of confluence for transfection. Cells were transfected with 1500 ng of pMJ920 (Cas9-GFP) and 500 ng of each sgRNA plasmid using a 1 DNA/3Fugene ratio of FuGENE HD (Promega, Madison, WI). For the minigene experiments, 1500 ng of mouse TTN-Mex2-6_V5 minigene was also added in the mixture. For GFP fluorescence-assisted cell sorting, a MoFlo (Beckman Coulter) was used.

Generation of the titin$^{Mex5-/Mex5-}$ mouse model

The *streptococcus pyogenes* SF370 derived Cas9 mRNA was purchased from TriLink Biotechnologies (L6125). The mRNA was purified using a Megaclear column and resuspended in EmbryoMax injection buffer (Temecula). The sgRNA was generated by *in vitro* transcription as previously published (36). Briefly, a PCR product was obtained by amplification from 20 ng of the sgRNA plasmid using Taq Phusion and a forward primer carrying an additional T7 promoter sequence on the 5' end (Supplementary Material, Table S1). After purification with the Qiaquick PCR product kit (Qiagen), the PCR template (150 ng) was used for *in vitro* transcription using the T7 Megashortscript T7 transcription kit (Life Technologies). The RNA was purified with the Megaclear kit (Life Technologies) and resuspended in EmbryoMax injection buffer. Both RNAs were quantified by Nanodrop and their purity was evaluated using an Agilent Small RNA Chip (Agilent).

Female B6/CBA F1 mice (C57Bl6NCr and CBA mice from Charles River laboratories, France) of approximately 6 weeks were superovulated by intraperitoneal injection of 5UI PMS (pregnant mare serum) and, 48 hrs later, 5UI hCG (human chorionic gonadotropin). Subsequently, they were mated with male B6/CBA F1 mice. Zygotes were isolated from the ampullae of the superovulated mice. After placing the embryos into M2 medium (Sigma, St Louis, USA), sgRNA and mRNA of spCas9 were co-injected at different concentrations (sgRNA: 10–20 ng/µl and Cas9 mRNA: 5-50 ng/µl) into the pronucleus using a microscope (Nikon, Tokyo, Japan) with micromanipulators (Narishige, London, UK), Vacutip holding pipettes (Eppendorf, Hamburg, Germany) and homemade injection pipettes prepared from borosilicate capillary glass (Harvard Apparatus, Holliston, USA). For injection, we used a Femtojet apparatus (Eppendorf, Hamburg, Germany). Approximately, 20 zygotes were reimplanted per pseudopregnant mouse immediately after injection.

All procedures performed on animals were in accordance with the European directive 2010/63/UE and were approved by the ethics committee (CECC003 C94-076-32) of the animal facility CNRS-SEAT-TAAM UPS44 under the number 1062. Animals were housed in a barrier facility with 12-hrs light, 12-hrs dark cycles, and provided food and water ad libitum. For histological and molecular analysis of mouse tissues, specimens were collected immediately after the confirmed death of the animal, snap frozen in liquid-nitrogen-cooled isopentane and stored at −80 °C.

Genomic DNA extraction and PCR assay for genomic deletions

DNA was extracted from cells two days after transfection using the DNeasy Blood and Tissue Kit (QIAGEN). Genomic mouse DNA was extracted from a small piece of tail or muscle using the same kit or the MagnaPure kit (Roche Life Science) according to the manufacturer's protocol. PCR on cellular DNA were performed with Phusion High-Fidelity DNA Polymerase (Thermo Scientific) and the following conditions: 98 °C for 30 sec, 30 cycles of 98 °C for 10 sec, 55 °C (genotyping) or 61 °C (off-target analysis) for 30 sec and 72 °C for 45 sec and a final extension of 72 °C for 5 min. PCR reactions on tail DNA were performed using KAPA2G Fast HotStart Genotyping PCR Kit with the same parameters as above (KAPABiosystems, KK5621). Detection of Mex5 deletions and inversions were performed using the primers mMex4.F/mMex6.R and mMex4.F/mMex5.F for cellular DNA) (Supplementary Material, Table S1) and with the primers inMex5.F/inMex6.R and inMex5.F/mMex5.F for tail DNA (Supplementary Material, Table S1). PCR primers were selected for PCR amplification of off-target sites with 2 mismatches (Supplementary Material, Table S3). NHEJ-repaired double-

strand breaks were determined after denaturation/renaturation using the T7 endonuclease 1 (Biolabs, M03025) as described (67). PCR amplicons were separated in Tris-Acetate EDTA (TAE)-agarose gel and stained with SYBR® Safe DNA gel stain (Life Technologies). For sequencing, the PCR amplicons were purified by the "NucleoSpin Gel and PCR Clean-up" kit (Macherey-Nagel).

mRNA analysis

Total RNA was extracted from C2 and minigene-transfected HER911 cells 48h post-transfection or from mouse muscle using TRIZOL (Life Technologies) according to the manufacturer's instructions. Residual DNA was removed from the samples using the Free DNA kit according to the manufacturer's protocol (Ambion). The quality of the purification was assessed by adding a control without reverse transcriptase in all experiments. Reverse transcription was performed using RevertAid H Minus Reverse Transcriptase (Life Technologies) according to the manufacturer's instructions.

For the analysis of the consequence of the Cas9 targeting at the RNA level, classical PCR analysis was performed using Phusion High-Fidelity DNA Polymerase (Thermo Scientific) or Herculase II Fusion DNA Polymerase (Agilent Genomics) and mMex4.F/mMex6.R primers (Supplementary Material, Table S1). The PCR products were size-verified and sequenced.

Real-time quantitative PCR was performed on 1 μg cDNA using ABI PRISM 7700 system (PE biosystems) with 0.2 μM of each primer and 0.1 μM of the probe according to the protocol Absolute QPCR Rox Mix (ABgene). Relative quantification of the Mex5+ isoform was performed using primers and Taqman probe located within Mex5 normalized to the level obtained with a PCR performed using primers and Taqman probe targeting the invariant Titin Mex2-3 region (Supplementary Material, Table S4). Calpain 3 RNA was quantified using the Mm00 482985_m1 Taqman gene expresssion assay (ThermoFisher). The ubiquitous acidic ribosomal phosphoprotein (P0) was used to normalize the data across samples. The primer pairs and Taqman probe used for P0 amplification were: m181PO.F (5′-CTCCAAGCAGATGCAGCAGA-3′), m267P0.R (5′-ACCATGATGCGC AAGGCCAT-3′) and m225P0.P (5′-CCGTGGTGCTGATGGGCAAGA A-3′). Each experiment was performed in duplicate.

For quantification of endogenous microRNA expression, 20 ng of total RNA extraction was reverse transcribed using the "TaqMan MicroRNA Reverse transcription" kit and subjected to PCR using MicroRNA Assays (Applied Biosystems). Normalization across samples was performed with the expression of snoRNA202 and miRNA-93. The following Taqman MicroRNA assays (Applied Biosystems).were used: assay ID0185 for miR-31, assay ID0464 for miR-142 3P, assay ID1232 for snoRNA202and assay ID1090 for mir-93.

Protein extraction and western blot analysis

To visualize the protein expressed from TTN-Mex2-6_V5 minigene in HER911 cells or to analyse muscle proteins from mice, total protein extraction was performed in a RIPA Lysis and Extraction Buffer (Thermo Scientific) and supplemented with Complete mini protease inhibitor cocktail (Roche). For titin western blot, muscle samples were homogenized using Ultra-Turrax and the cytoskeletal fraction was obtained with the ProteoExtract® Subcellular Proteome Extraction Kit (S-PEK, Calbiochem, Germany). These experimental conditions led to controlled proteolysis of Titin, allowing detection of specific bands by western blot using C-ter titin antibodies. Protein extracts were mixed with LDS NuPAGE Buffer (Life Technologies) supplemented with 100 mM DTT, denatured at 70 °C for 10 min and loaded on a 4-12% Bis-Tris gel (Invitrogen). After migration in MES Buffer (Invitrogen), transfer to nitrocelullose membranes (Invitrogen) was performed in iBlot® Gel Transfer Stacks (Life Technologies) according to the manufacturer's instructions. After blotting, the membranes were probed with different antibodies. Mouse primary antibody anti-V5 (Life technologies, PN 46-1157, dilution 1:750) and rabbit primary antibody anti-GFP (Abcam, ab6556, dilution 1:500) were used to detect TTN-Mex2-6_V5 minigene protein and Cas9-GFP, respectively, in the *in vitro* experiment. Detection of titin band *in vivo* was performed using a rabbit polyclonal is7 (dilution 1:100) antibody that we generated by three successive injections of 2 mg of the LVEEPPPREVVLKTSC peptide from mouse is7 domain (production and purification according to the PolyExpress Custom Polyclonal antibody basic package, Genscript, Piscataway, USA). Detection of calpain 3, CARP and MURF1/MURF2 were performed using calpain 3 (Novocastra, NCLCALP-12A2, dilution 1:200), CARP (Proteintech, 11427.1.AP, dilution 1:500), MURF1 (Abcam, ab77577, dilution 1:500), MURF2 (Abcam, ab4125, dilution 1:500) mouse monoclonal antibodies. α-actin (A-2066, Sigma, rabbit antibody, dilution 1:500) and β-actin (Sigma, A1978, dilution 1:500) were used to normalize protein load across samples. Fluorescent detection was performed using secondary antibodies with IRDye for revelation by the infrared scanner Odyssey (LI-COR, Biosciences, Lincoln, NE).

Histology and immunohistochemistry

Longitudinal and transverse cryosections (8 or 10 μm thickness) were prepared from frozen muscles and were processed for Hematoxylin-Phloxine-Saffron (HPS) or Sirius Red histological stainings. Digital images were captured with a CCD camera (Sony).

The antibodies used for immuno-staining on *gastrocnemius* or *Tibialis Anterior* muscles are Titin rabbit m10-1 (25) (dilution 1:4), rabbit is7 (dilution 1:4), mouse m8-9 (dilution 1:40), N2A (US biological, T5650, dilution 1:40) and PEVK (Developmental Studies Hybridoma Bank, 9D10, dilution 1:50) antibodies. For titin partners, the antibodies used were directed against CAPN3 (Triple Point, RP4, dilution 1:40), MURF1, MURF2, CARP and OBSCN (dilution 1:60). Primary antibody incubations were followed by 1 hour incubation with Alexa 488 or 594 goat secondary antibodies (Life Technologies, 1:1000) from the adequate species. A solution containing Tween 0.1% was used to wash the is7 antibody during the staining. Sections were mounted in Fluoromount G (SouthernBiotech, Birmingham, USA) and examined through a Leica confocal microscope (TCS SP2.AOBS microscope, Leica, Germany) using the 488nm and the 594 nm lines of an argon laser.

In vitro evaluation of muscle function

Animals were anaesthetized by intraperitoneal injection of pentobarbital (100 mg/kg). The muscles were surgically excised and maintained in Krebs buffer. Measurement of isometric contractile properties was performed on *Soleus* muscle according to methods previously described.

Statistical analysis

Analysis of the Mendelian transmission ratio was performed using the χ^2 test. Individual means and distributions were

compared using the Mann-Whitney and the Kolmogorov-Smirnov non-parametric tests, respectively. The *p*-value of less than 0.05 was considered significant.

Supplementary Material

Supplementary Material is available at *HMG* online.

Acknowledgements

The authors thank Bjarne Udd for TTN antibodies and the team from SEAT-TAAM Phenomin CNRS. We also acknowledge Pr. Jennifer A. Doudna (University of California) and Dr J. Keith Joung (Massachusetts General Hospital) for the Cas9 and sgRNA plasmids, respectively. We would like to thank all the DDC team members for their constant help and support.

Conflict of Interest statement. None declared.

Funding

The study was supported by the Association Française contre les Myopathies and a grant from the Fondation Leducq.

References

1. Pan, Q., Shai, O., Lee, L.J., Frey, B.J. and Blencowe, B.J. (2008) Deep surveying of alternative splicing complexity in the human transcriptome by high-throughput sequencing. *Nat. Genet.*, **40**, 1413–1415.
2. Wang, E.T., Sandberg, R., Luo, S., Khrebtukova, I., Zhang, L., Mayr, C., Kingsmore, S.F., Schroth, G.P. and Burge, C.B. (2008) Alternative isoform regulation in human tissue transcriptomes. *Nature*, **456**, 470–476.
3. Modrek, B. and Lee, C. (2002) A genomic view of alternative splicing. *Nat Genet*, **30**, 13–19.
4. Tress, M.L., Martelli, P.L., Frankish, A., Reeves, G.A., Wesselink, J.J., Yeats, C., Olason, P.I., Albrecht, M., Hegyi, H., Giorgetti, A., *et al.* (2007) The implications of alternative splicing in the ENCODE protein complement. *Proc. Natl Acad. Sci. U S A*, **104**, 5495–5500.
5. Frankish, A., Mudge, J.M., Thomas, M. and Harrow, J. (2012) The importance of identifying alternative splicing in vertebrate genome annotation. *Database (Oxford)*, **2012**, bas014.
6. Takeda, J., Suzuki, Y., Sakate, R., Sato, Y., Gojobori, T., Imanishi, T. and Sugano, S. (2010) H-DBAS: human-transcriptome database for alternative splicing: update 2010. *Nucleic Acids Res.*, **38**, D86–D90.
7. Lee, J.S., Kallehauge, T.B., Pedersen, L.E. and Kildegaard, H.F. (2015) Site-specific integration in CHO cells mediated by CRISPR/Cas9 and homology-directed DNA repair pathway. *Sci. Rep.*, **5**, 8572.
8. Maniatis, T. and Tasic, B. (2002) Alternative pre-mRNA splicing and proteome expansion in metazoans. *Nature*, **418**, 236–243.
9. Breitbart, R.E., Andreadis, A. and Nadal-Ginard, B. (1987) Alternative splicing: a ubiquitous mechanism for the generation of multiple protein isoforms from single genes. *Annu. Rev. Biochem.*, **56**, 467–495.
10. Mele, M., Ferreira, P.G., Reverter, F., DeLuca, D.S., Monlong, J., Sammeth, M., Young, T.R., Goldmann, J.M., Pervouchine, D.D., Sullivan, T.J., *et al.* (2015) Human genomics. The human transcriptome across tissues and individuals. *Science*, **348**, 660–665.
11. Chabot, B. and Shkreta, L. (2016) Defective control of pre-messenger RNA splicing in human disease. *J. Cell Biol.*, **212**, 13–27.
12. Bang, M.L., Centner, T., Fornoff, F., Geach, A.J., Gotthardt, M., McNabb, M., Witt, C.C., Labeit, D., Gregorio, C.C., Granzier, H., *et al.* (2001) The complete gene sequence of titin, expression of an unusual approximately 700-kDa titin isoform, and its interaction with obscurin identify a novel Z-line to I-band linking system. *Circ. Res.*, **89**, 1065–1072.
13. Jackel, M., Witt, C., Antonova, O., Curdt, I., Labeit, S. and Jockusch, H. (1997) Deletion in the Z-line region of the titin gene in a baby hamster kidney cell line, BHK-21-Bi. *FEBS Lett.*, **408**, 21–24.
14. Labeit, S. and Kolmerer, B. (1995) Titins: giant proteins in charge of muscle ultrastructure and elasticity. *Science*, **270**, 293–296.
15. Gregorio, C.C., Trombitas, K., Centner, T., Kolmerer, B., Stier, G., Kunke, K., Suzuki, K., Obermayr, F., Herrmann, B., Granzier, H., *et al.* (1998) The NH2 terminus of titin spans the Z-disc: its interaction with a novel 19-kD ligand (T-cap) is required for sarcomeric integrity. *J. Cell Biol.*, **143**, 1013–1027.
16. Obermann, W.M., Gautel, M., Weber, K. and Furst, D.O. (1997) Molecular structure of the sarcomeric M band: mapping of titin and myosin binding domains in myomesin and the identification of a potential regulatory phosphorylation site in myomesin. *Embo J.*, **16**, 211–220.
17. Cazorla, O., Freiburg, A., Helmes, M., Centner, T., McNabb, M., Wu, Y., Trombitas, K., Labeit, S. and Granzier, H. (2000) Differential expression of cardiac titin isoforms and modulation of cellular stiffness. *Circ. Res.*, **86**, 59–67.
18. Labeit, S., Lahmers, S., Burkart, C., Fong, C., McNabb, M., Witt, S., Witt, C., Labeit, D. and Granzier, H. (2006) Expression of distinct classes of titin isoforms in striated and smooth muscles by alternative splicing, and their conserved interaction with filamins. *J. Mol. Biol.*, **362**, 664–681.
19. Neagoe, C., Opitz, C.A., Makarenko, I. and Linke, W.A. (2003) Gigantic variety: expression patterns of titin isoforms in striated muscles and consequences for myofibrillar passive stiffness. *J. Muscle Res. Cell Motil.*, **24**, 175–189.
20. Kolmerer, B., Olivieri, N., Witt, C.C., Herrmann, B.G. and Labeit, S. (1996) Genomic organization of M line titin and its tissue-specific expression in two distinct isoforms. *J. Mol. Biol.*, **256**, 556–563.
21. Guo, W., Bharmal, S.J., Esbona, K. and Greaser, M.L. (2010) Titin diversity–alternative splicing gone wild. *J. Biomed. Biotechnol.*, **2010**, 753675.
22. Duguez, S., Bartoli, M. and Richard, I. (2006) Calpain 3: a key regulator of the sarcomere? *Febs J.*, **273**, 3427–3436.
23. Richard, I., Broux, O., Allamand, V., Fougerousse, F., Chiannilkulchai, N., Bourg, N., Brenguier, L., Devaud, C., Pasturaud, P., Roudaut, C., *et al.* (1995) Mutations in the proteolytic enzyme calpain 3 cause limb-girdle muscular dystrophy type 2A. *Cell*, **81**, 27–40.
24. Charton, K., Daniele, N., Vihola, A., Roudaut, C., Gicquel, E., Monjaret, F., Tarrade, A., Sarparanta, J., Udd, B. and Richard, I. (2010) Removal of the calpain 3 protease reverses the myopathology in a mouse model for titinopathies. *Hum. Mol. Genet.*, **19**, 4608–4624.
25. Charton, K., Sarparanta, J., Vihola, A., Milic, A., Jonson, P.H., Suel, L., Luque, H., Boumela, I., Richard, I. and Udd, B. (2015) CAPN3-mediated processing of C-terminal titin replaced by pathological cleavage in titinopathy. *Hum. Mol. Genet.*, **24**, 3718–3731.

26. Sarparanta, J., Blandin, G., Charton, K., Vihola, A., Marchand, S., Milic, A., Hackman, P., Ehler, E., Richard, I. and Udd, B. (2010) Interactions with M-band titin and calpain 3 link myospryn (CMYA5) to tibial and limb-girdle muscular dystrophies. *J. Biol. Chem.*, **285**, 30304–30315.
27. Ojima, K., Kawabata, Y., Nakao, H., Nakao, K., Doi, N., Kitamura, F., Ono, Y., Hata, S., Suzuki, H., Kawahara, H., *et al.* (2010) Dynamic distribution of muscle-specific calpain in mice has a key role in physical-stress adaptation and is impaired in muscular dystrophy. *J. Clin. Invest.*, **120**, 2672–2683.
28. Ojima, K., Ono, Y., Hata, S., Koyama, S., Doi, N. and Sorimachi, H. (2005) Possible functions of p94 in connectin-mediated signaling pathways in skeletal muscle cells. *J. Muscle. Res. Cell Motil*, **26**, 409–417.
29. Beckmann, J.S. and Spencer, M. (2008) Calpain 3, the "gatekeeper" of proper sarcomere assembly, turnover and maintenance. *Neuromuscul. Disord.*, **18**, 913–921.
30. Ono, Y., Torii, F., Ojima, K., Doi, N., Yoshioka, K., Kawabata, Y., Labeit, D., Labeit, S., Suzuki, K., Abe, K., *et al.* (2006) Suppressed disassembly of autolyzing p94/CAPN3 by N2A connectin/titin in a genetic reporter system. *J. Biol. Chem.*, **281**, 18519–18531.
31. Sorimachi, H., Kinbara, K., Kimura, S., Takahashi, M., Ishiura, S., Sasagawa, N., Sorimachi, N., Shimada, H., Tagawa, K., Maruyama, K., *et al.* (1995) Muscle-specific calpain, p94, responsible for limb girdle muscular dystrophy type 2A, associates with connectin through IS2, a p94-specific sequence. *J. Biol. Chem.*, **270**, 31158–31162.
32. Hackman, P., Marchand, S., Sarparanta, J., Vihola, A., Penisson-Besnier, I., Eymard, B., Pardal-Fernandez, J.M., Hammouda el, H., Richard, I., Illa, I., *et al.* (2008) Truncating mutations in C-terminal titin may cause more severe tibial muscular dystrophy (TMD). *Neuromuscul. Disord.*, **18**, 922–928.
33. Lin, X., Miller, J.W., Mankodi, A., Kanadia, R.N., Yuan, Y., Moxley, R.T., Swanson, M.S. and Thornton, C.A. (2006) Failure of MBNL1-dependent post-natal splicing transitions in myotonic dystrophy. *Hum. Mol. Genet.*, **15**, 2087–2097.
34. Kinbara, K., Sorimachi, H., Ishiura, S. and Suzuki, K. (1997) Muscle-specific calpain, p94, interacts with the extreme C-terminal region of connectin, a unique region flanked by two immunoglobulin C2 motifs. *Arch. Biochem. Biophys.*, **342**, 99–107.
35. Fu, Y., Reyon, D. and Joung, J.K. (2014) Targeted genome editing in human cells using CRISPR/Cas nucleases and truncated guide RNAs. *Methods Enzymol.*, **546**, 21–45.
36. Yang, H., Wang, H. and Jaenisch, R. (2014) Generating genetically modified mice using CRISPR/Cas-mediated genome engineering. *Nat. Protoc.*, **9**, 1956–1968.
37. Greco, S., De Simone, M., Colussi, C., Zaccagnini, G., Fasanaro, P., Pescatori, M., Cardani, R., Perbellini, R., Isaia, E., Sale, P., *et al.* (2009) Common micro-RNA signature in skeletal muscle damage and regeneration induced by Duchenne muscular dystrophy and acute ischemia. *Faseb J.*, **23**, 3335–3346.
38. Fordham, J.B., Naqvi, A.R. and Nares, S. (2015) Regulation of miR-24, miR-30b, and miR-142-3p during macrophage and dendritic cell differentiation potentiates innate immunity. *J. Leukoc. Biol.*, **98**, 195–207.
39. Radke, M.H., Peng, J., Wu, Y., McNabb, M., Nelson, O.L., Granzier, H. and Gotthardt, M. (2007) Targeted deletion of titin N2B region leads to diastolic dysfunction and cardiac atrophy. *Proc. Natl Acad. Sci. U S A*, **104**, 3444–3449.
40. Granzier, H.L., Radke, M.H., Peng, J., Westermann, D., Nelson, O.L., Rost, K., King, N.M., Yu, Q., Tschope, C., McNabb, M., *et al.* (2009) Truncation of titin's elastic PEVK region leads to cardiomyopathy with diastolic dysfunction. *Circ. Res.*, **105**, 557–564.
41. Parra, M.K., Gee, S., Mohandas, N. and Conboy, J.G. (2011) Efficient in vivo manipulation of alternative pre-mRNA splicing events using antisense morpholinos in mice. *J. Biol. Chem.*, **286**, 6033–6039.
42. Fugier, C., Klein, A.F., Hammer, C., Vassilopoulos, S., Ivarsson, Y., Toussaint, A., Tosch, V., Vignaud, A., Ferry, A., Messaddeq, N., *et al.* (2011) Misregulated alternative splicing of BIN1 is associated with T tubule alterations and muscle weakness in myotonic dystrophy. *Nat. Med.*, **17**, 720–725.
43. Rau, F., Laine, J., Ramanoudjame, L., Ferry, A., Arandel, L., Delalande, O., Jollet, A., Dingli, F., Lee, K.Y., Peccate, C., *et al.* (2015) Abnormal splicing switch of DMD's penultimate exon compromises muscle fibre maintenance in myotonic dystrophy. *Nat. Commun.*, **6**, 7205.
44. Huang, C., Zhou, Q., Liang, P., Hollander, M.S., Sheikh, F., Li, X., Greaser, M., Shelton, G.D., Evans, S. and Chen, J. (2003) Characterization and in vivo functional analysis of splice variants of cypher. *J. Biol. Chem.*, **278**, 7360–7365.
45. Spencer, M.J., Guyon, J.R., Sorimachi, H., Potts, A., Richard, I., Herasse, M., Chamberlain, J., Dalkilic, I., Kunkel, L.M. and Beckmann, J.S. (2002) Stable expression of calpain 3 from a muscle transgene in vivo: immature muscle in transgenic mice suggests a role for calpain 3 in muscle maturation. *Proc. Natl Acad. Sci .U S A*, **99**, 8874–8879.
46. Guo, W., Schafer, S., Greaser, M.L., Radke, M.H., Liss, M., Govindarajan, T., Maatz, H., Schulz, H., Li, S., Parrish, A.M., *et al.* (2012) RBM20, a gene for hereditary cardiomyopathy, regulates titin splicing. *Nat. Med.*, **18**, 766–773.
47. Dixon, D.M., Choi, J., El-Ghazali, A., Park, S.Y., Roos, K.P., Jordan, M.C., Fishbein, M.C., Comai, L. and Reddy, S. (2015) Loss of muscleblind-like 1 results in cardiac pathology and persistence of embryonic splice isoforms. *Sci. Rep.*, **5**, 9042.
48. Wang, H., Yang, H., Shivalila, C.S., Dawlaty, M.M., Cheng, A.W., Zhang, F. and Jaenisch, R. (2013) One-step generation of mice carrying mutations in multiple genes by CRISPR/Cas-mediated genome engineering. *Cell*, **153**, 910–918.
49. Fujii, W., Onuma, A., Sugiura, K. and Naito, K. (2014) One-step generation of phenotype-expressing triple-knockout mice with heritable mutated alleles by the CRISPR/Cas9 system. *J. Reprod. Dev.*, **60**, 324–327.
50. Young, C.S., Hicks, M.R., Ermolova, N.V., Nakano, H., Jan, M., Younesi, S., Karumbayaram, S., Kumagai-Cresse, C., Wang, D., Zack, J.A., *et al.* (2016) A single CRISPR-Cas9 deletion strategy that targets the majority of DMD patients restores dystrophin function in hiPSC-derived muscle cells. *Cell Stem Cell*, in press.
51. Slaymaker, I.M., Gao, L., Zetsche, B., Scott, D.A., Yan, W.X. and Zhang, F. (2016) Rationally engineered Cas9 nucleases with improved specificity. *Science*, **351**, 84–88.
52. Kleinstiver, B.P., Pattanayak, V., Prew, M.S., Tsai, S.Q., Nguyen, N.T., Zheng, Z. and Joung, J.K. (2016) High-fidelity CRISPR-Cas9 nucleases with no detectable genome-wide off-target effects. *Nature*, **529**, 490–495.
53. Udd, B. (1992) Limb-girdle type muscular dystrophy in a large family with distal myopathy: homozygous manifestation of a dominant gene? *J. Med. Genet.*, **29**, 383–389.
54. Erickson, H.P. (1994) Reversible unfolding of fibronectin type III and immunoglobulin domains provides the structural

basis for stretch and elasticity of titin and fibronectin. *Proc. Natl Acad. Sci. U S Aa*, **91**, 10114–10118.
55. Sjostrom, M. and Squire, J.M. (1977) Fine structure of the A-band in cryo-sections. The structure of the A-band of human skeletal muscle fibres from ultra-thin cryo-sections negatively stained. *J. Mol. Biol.*, **109**, 49–68.
56. Edman, A.C., Squire, J.M. and Sjostrom, M. (1988) Fine structure of the A-band in cryo-sections. Diversity of M-band structure in chicken breast muscle. *J. Ultrastruct. Mol. Struct. Res.*, **100**, 1–12.
57. Podlubnaya, Z.A., Shpagina, M.D. and Lednev, V.V. (1989) Manifestation of the stripes of minor proteins location in A-bands of rabbit cardiac myofibrils. *J. Mol. Biol.*, **210**, 655–658.
58. Carlsson, E. and Thornell, L.E. (1987) Diversification of the myofibrillar M-band in rat skeletal muscle during postnatal development. *Cell Tissue Res.*, **248**, 169–180.
59. Herasse, M., Ono, Y., Fougerousse, F., Kimura, E., Stockholm, D., Beley, C., Montarras, D., Pinset, C., Sorimachi, H., Suzuki, K., *et al*. (1999) Expression and functional characteristics of calpain 3 isoforms generated through tissue-specific transcriptional and posttranscriptional events. *Mol. Cell Biol.*, **19**, 4047–4055.
60. Hayashi, C., Ono, Y., Doi, N., Kitamura, F., Tagami, M., Mineki, R., Arai, T., Taguchi, H., Yanagida, M., Hirner, S., *et al*. (2008) Multiple molecular interactions implicate the connectin/titin N2A region as a modulating scaffold for p94/calpain 3 activity in skeletal muscle. *J. Biol. Chem.*, **283**, 14801–14814.
61. Laure, L., Suel, L., Roudaut, C., Bourg, N., Ouali, A., Bartoli, M., Richard, I. and Daniele, N. (2009) Cardiac ankyrin repeat protein is a marker of skeletal muscle pathological remodelling. *Febs J.*, **276**, 669–684.
62. Sander, J.D., Zaback, P., Joung, J.K., Voytas, D.F. and Dobbs, D. (2007) Zinc Finger Targeter (ZiFiT): an engineered zinc finger/target site design tool. *Nucleic Acids Res.*, **35**, W599–W605.
63. Sander, J.D., Maeder, M.L., Reyon, D., Voytas, D.F., Joung, J.K. and Dobbs, D. (2010) ZiFiT (Zinc Finger Targeter): an updated zinc finger engineering tool. *Nucleic Acids Res.*, **38**, W462–W468.
64. Wang, T., Wei, J.J., Sabatini, D.M. and Lander, E.S. (2014) Genetic screens in human cells using the CRISPR-Cas9 system. *Science*, **343**, 80–84.
65. Jinek, M., East, A., Cheng, A., Lin, S., Ma, E. and Doudna, J. (2013) RNA-programmed genome editing in human cells. *Elife*, **2**, e00471.
66. Monjaret, F., Bourg, N., Suel, L., Roudaut, C., Le Roy, F, Richard, I. and Charton, K., (2014) CIS-splicing and translation of the pre-trans-splicing molecule combine with efficiency in spliceosome-mediated RNA trans-splicing. *Mol Ther*, **22**, 1176–1187.
67. Holkers, M., Cathomen, T. and Goncalves, M.A. (2014) Construction and characterization of adenoviral vectors for the delivery of TALENs into human cells. *Methods*, **69**, 179–187.